Electron and X-ray Diffraction from Antiphase Domains in the Barium Magnesium Hollandite $Ba_{1\cdot33}Mg_{1\cdot33}Ti_{6\cdot67}O_{16}$

By Robert W. Cheary and Roseanne Squadrito

School of Physical Sciences, University of Technology, Sydney, Broadway, New South Wales, Australia 2007

Abstract

The barium hollandite $Ba_{1\cdot33}Mg_{1\cdot33}Ti_{6\cdot67}O_{16}$ undergoes an order–disorder transition at 1100 (10) K. Below this temperature the Ba and vacant sites in the tunnels of the hollandite structure are ordered with the sequence Ba–Ba–vacancy and $b = 3b_{hollandite}$. At the same time, antiphase domains form which produce broadened X-ray diffraction lines and electron diffraction peaks shifted off their commensurate superstructure positions. This shift in the diffraction peaks is explained by the formation of a boundary layer with a spacing of $2\cdot5b_{hollandite}$ between adjacent domains. Equations are developed relating the peak shift to the domain size which are consistent with observed electron diffraction patterns. The theory is extended to interpret the broadening of X-ray powder diffraction lines. During the early stages of domain growth boundaries form on (101), (10$\bar{1}$) and (010) planes. Domain growth occurs mainly in the [101] and [10$\bar{1}$] directions and after extended annealing only (010) boundaries remain.

Introduction

Barium hollandite is one component of the synthetic mineral SYNROC. This material is being developed to immobilize high-level nuclear waste (Fielding & White, 1987) with hollandite acting as the host for radioactive caesium, barium and other large alkali ions. Kesson & White (1986*a*, *b*) and Cheary (1987) have examined how these ions are accommodated within the hollandite structure and the nature of the ordering that occurs amongst these ions on the tunnel sites. In barium magnesium hollandites, the subject of the present work, the tunnel sites are only partially occupied by Ba and the monoclinic unit cell (*b* axis unique) has the composition

$$[Ba_x \otimes_{2-x}][Mg_x Ti_{8-x}]O_{16}$$

where $\otimes$ represents vacant sites within the tunnels and x can be any value between 1·14 (57% occupancy) and 1·33 (67% occupancy). The Mg and Ti ions occupy sites within oxygen octahedra that form the tunnel walls and the tunnel axis is along the *b* direction.

Various ordered sequences or superstructures of Ba and $\otimes$ can form depending on the composition but only at $x = 1\cdot20$ and 1·33 are the superstructures commensurate with the hollandite lattice (Bursill & Grzinic, 1980). At $x = 1\cdot33$ the ordering sequence is Ba–Ba–$\otimes$ and the superstructure has a repeat distance along the tunnel direction $b_{sup} = 3b_{hol}$ where $b_{hol} \simeq 3$ Å is the hollandite unit-cell parameter along the tunnel direction. At $x = 1\cdot20$ the sequence adopted is Ba–Ba–$\otimes$–Ba–$\otimes$ and $b_{sup} = 5b_{hol}$. Ordering is readily identified by the presence of superlattice peaks in both the electron diffraction pattern and X-ray powder pattern. In electron diffraction the multiplicity m of the ordering can be measured directly from a [100] or [001] zone pattern by measuring the ratio of the height of the first layer of superlattice spots to the height of the 020 spot above the zero layer. Perfect ordering at $x = 1\cdot20$ and 1·33 therefore corresponds to multiplicities of $m = 5$ and 6, respectively. The variation of multiplicity with Ba concentration has been measured by Bursill & Grzinic (1980) and Cheary & Squadrito (1989). At the lower end of the solid-solution range of barium magnesium hollandites (*i.e.* $x = 1\cdot14$), the multiplicity is in the range 4·70–4·75. It should be noted that Bursill & Grzinic ascribe their minimum multiplicity to a composition of $x = 0\cdot8$. We believe this to be incorrect as the minimum x value has been clearly established as $x \simeq 1\cdot14$ (Roth, 1981; Cheary & Squadrito, 1989). This is further supported by the fact that no Ba hollandites have been synthesized with $x < 1$ (Kesson & White, 1986*a*). At the upper end of the Ba concentration range, $x = 1\cdot33$, the multiplicity reaches a maximum between 5·85 and 5·90 even with excess Ba in the starting materials. In $Ba_{1\cdot33}(Ga/Ti)$ hollandite the maximum observed multiplicity by Bursill & Grzinic is 5·93. In general, the multiplicity m and the Ba/unit cell x closely follow the relation proposed by Mijlhoff, IJdo & Zandbergen (1985),

$$x = 2(1 - 2/m). \qquad (1)$$

As shown in Cheary & Squadrito (1989), (1) works well in the middle of the composition range but is only approximate at either end of the solid-solution range. At the $x = 1\cdot33$ end in particular the observed multiplicity is invariably about 0·1 less than the predicted value of 6. Fig. 1 demonstrates the form of the

　　　　© 1992 International Union of Crystallography

electron diffraction pattern normally observed from $Ba_{1.33}Mg_{1.33}Ti_{6.67}O_{16}$ with the superlattice spots indexed on a hollandite lattice. When $h + l =$ even the most intense superlattice peaks for $k < 1$ occur at $k = \frac{1}{3} + \varepsilon_0$ and the less intense at $k = \frac{2}{3} + \varepsilon_0$ where $\varepsilon_0 = (2/m - 1/3) \simeq 0 \cdot 01$. Superlattice peaks also form at $k = \frac{1}{3} + \varepsilon_0$ and $\frac{2}{3} + \varepsilon_0$ when $h + l$ is odd but $\varepsilon_0 \simeq -0 \cdot 01$ and the most intense peak is at $k \simeq \frac{2}{3}$.

It was suggested by Cheary & Squadrito (1989) that the deviation from the $3b_{hol}$ superstructure for $x = 1 \cdot 33$ is related to the formation of antiphase domains. Microdomains in hollandites were first noted by Bursill & Grzinic (1980) and the concept of intergrowths of domains of $3b_{hol}$ and $5b_{hol}$ order was used to explain qualitatively the variation of the observed multiplicities between $x = 1 \cdot 2$ and $x = 1 \cdot 33$. The existence of antiphase domains in hollandites was first discussed by Fanchon, Vicat, Hodeau, Wolfers, Tran Qui & Strobel (1987) in their study of $Ba_{1.2}Mg_{1.2}Ti_{6.8}O_{16}$. In this compound it was noted that large domains with a $5b_{hol}$ superstructure contain smaller domains also with $5b_{hol}$ superstructures but shifted with respect to one another at the domain walls. We believe this is also the case in $x = 1 \cdot 33$ hollandites within $3b_{hol}$ domains. In Bursill & Grzinic (1980) the ordered domains illustrated in the electron micrograph for an $x = 1 \cdot 33$ specimen are regions of perfect $3b_{hol}$ order typically 20 to 60 Å in size in the tunnel direction. It is proposed that the superstructure in an $x = 1 \cdot 33$ hollandite changes from the sequence $Ba-Ba-\otimes$ in one domain to $\otimes-Ba-Ba$ or $Ba-\otimes-Ba$ in an adjacent domain. With antiphase domains ~ 50 Å in length, the disruption to the $3b_{hol}$ periodicity at the boundaries between domains will be enough to reduce the multiplicity from 6 to the usual observed value of $5 \cdot 80$ to $5 \cdot 90$ in $Ba_{1.33}Mg_{1.33}Ti_{6.67}O_{16}$.

The presence of these antiphase domains indicates that the ordering of the Ba ions is incomplete. This situation is similar to that found in Cu_3Au alloy which forms antiphase domains once the temperature drops below the order-disorder transition (Warren, 1969). The change from partial order to complete order

occurs through the growth of these domains. The similarity to Cu_3Au implies that an order-disorder transition also exists amongst the Ba ions in Ba hollandites. This has in fact proved to be correct and an order-disorder transition of the Ba ions has since been measured by us in $Ba_{1.33}Mg_{1.33}Ti_{6.67}O_{16}$ at 1100 (10) K. This was done by examining the intensity of the strongest X-ray superlattice line with increasing temperature and determining the temperature at which it disappeared. The formation and growth of the antiphase domains can be examined by analysing the position and breadth of the superlattice lines when a specimen is subject to different heat treatment procedures. Figs. 2(a), (b) and (c) are different parts of X-ray powder patterns from a single specimen of $Ba_xMg_xTi_{8-x}O_{16}$ ($x \simeq 1 \cdot 33$) at different stages in the ordering process. In the lower pattern in each of Figs. 2(a), (b) and (c), the specimen was cooled rapidly from 1230 K to room temperature over a 2 h period and only limited domain growth occurred. This shows as broadening of the superlattice lines relative to the hollandite lattice lines. The upper patterns in Figs. 2(a), (b) and (c) correspond to the same specimen after being reheated to 1060 K (i.e. just below the transition temperature) and annealed for 160 h to allow the domains to grow. As expected, the superlattice lines become sharper and they also shift to 2θ values corresponding to a larger multiplicity value (see Fig. 2c). Throughout the heat treatment the 2θ values and the relative intensities of hollandite lattice lines are substantially unchanged.

The purpose of the present paper is to develop a diffraction theory for relating the observed multiplicity of the superlattice peaks in an electron diffraction pattern from $Ba_{1.33}Mg_{1.33}Ti_{6.67}O_{16}$ to the size of the antiphase domains and the structure at the boundaries between the domains. This is essentially a one-dimensional problem as the multiplicity is given from the intensity distribution along the b^* direction at each integral value of h and l. The theory is generalized to reflect the three-dimensional domain structure so that it can be applied to X-ray powder diffraction data. This will allow validity of the theory to be tested more rigorously through an analysis of the breadth of each superlattice line as well as its shift relative the perfectly ordered 2θ position.

Description of the antiphase domain model

In the present analysis we have assumed substitutional disorder of the Mg/Ti ions on the octahedral sites. Fanchon et al. (1987) found no evidence for ordering of these ions in single-crystal X-ray data from $Ba_{1.2}Mg_{1.2}Ti_{6.8}O_{16}$ and noted that $I2/m$ symmetry does not predict any simple form of ordering. Cheary & Squadrito (1989) found that the ratio of Mg/Ti on each of the octahedral sites is different, but in each case the ions are substitutionally disor-
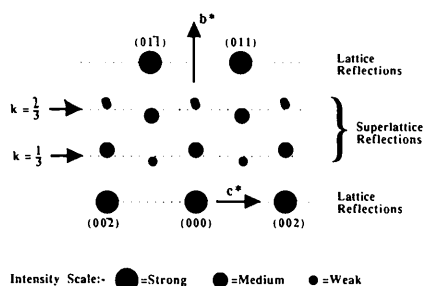

Fig. 1. A diagram of the [100] zone electron diffraction pattern from $Ba_{1.33}Mg_{1.33}Ti_{6.67}O_{16}$ hollandite showing the zig-zag pattern of superlattice lines. For a scheme of indexing based on a hollandite lattice, a perfect $3b$ superstructure would produce superlattice lines with $k = 1/3$ or $2/3$.

dered on their respective sites. Even though the occupancy of the Mg and Ti atoms is different on the two sets of octahedral sites there does not appear to be any long-range ordering of these ions. In this work the contribution of Mg and Ti to the superstructure reflections is assumed to be negligible. This being the case, the intensity distribution of the superlattice lines depends only on the Ba ions and the atomic coordinates of the ordered sequence of these ions and vacancies in the tunnels. Within each hollandite unit cell there are two tunnel sites with centres at 0,0,0 and $\frac{1}{2},\frac{1}{2},\frac{1}{2}$. These sites are in separate but parallel tunnels which run in the y direction (*i.e.* the b axis). The Ba–Ba–$\otimes$ ordering within each tunnel results in the Ba ions being pushed slightly off centre in the tunnel direction. This arises from mutual electrostatic repulsion between neighbouring pairs of Ba ions. Two structural constraints have been identified which control the local ordering of the Ba ions and vacancies in hollandites. The first of these is that vacancies never occupy adjacent sites along a tunnel (Mijlhoff *et al.*, 1985). Secondly, vacancies in adjacent parallel tunnels always occur in pairs and form unbroken corrugated layers parallel to the (010) plane (Fanchon

et al., 1987). These rules mean that if a vacancy exists at 0,0,0 then the adjacent sites in the same tunnel at 0,1,0 and 0,–1,0 will be occupied by Ba ions. Also, in the adjacent tunnel one of the sites at either $\frac{1}{2},\frac{1}{2},\frac{1}{2}$ or $\frac{1}{2},-\frac{1}{2},\frac{1}{2}$ will be vacant.

In the present work we will classify the two types of vacancy pairing in adjacent tunnels as $\Uparrow$ pairs when the two coordinates are 0,0,0 and $\frac{1}{2},\frac{1}{2},\frac{1}{2}$ and $\Downarrow$ pairs when these coordinates are 0,0,0 and $\frac{1}{2},-\frac{1}{2},\frac{1}{2}$. Six possible $3b$ supercells can be formed from these vacancies, three based on $\Uparrow$ vacancy pairs termed A, B and C cells and three based on $\Downarrow$ vacancy pairs termed $A\#$, $B\#$ and $C\#$ cells. These are shown in Fig. 3. Each of these supercells is the same except for an origin shift or a twofold rotation about the b axis. As there are six possible supercells there will also be six possible types of antiphase domain. At the boundary between two domains the structure must still satisfy the condition that vacancies cannot exist as nearest neighbours in a tunnel. This automatically limits the way a changeover can occur at a boundary. Fig. 4(a) illustrates four possible single-layer boundary types going from an A-type cell to one of the other types. Within each domain the vacancy layers
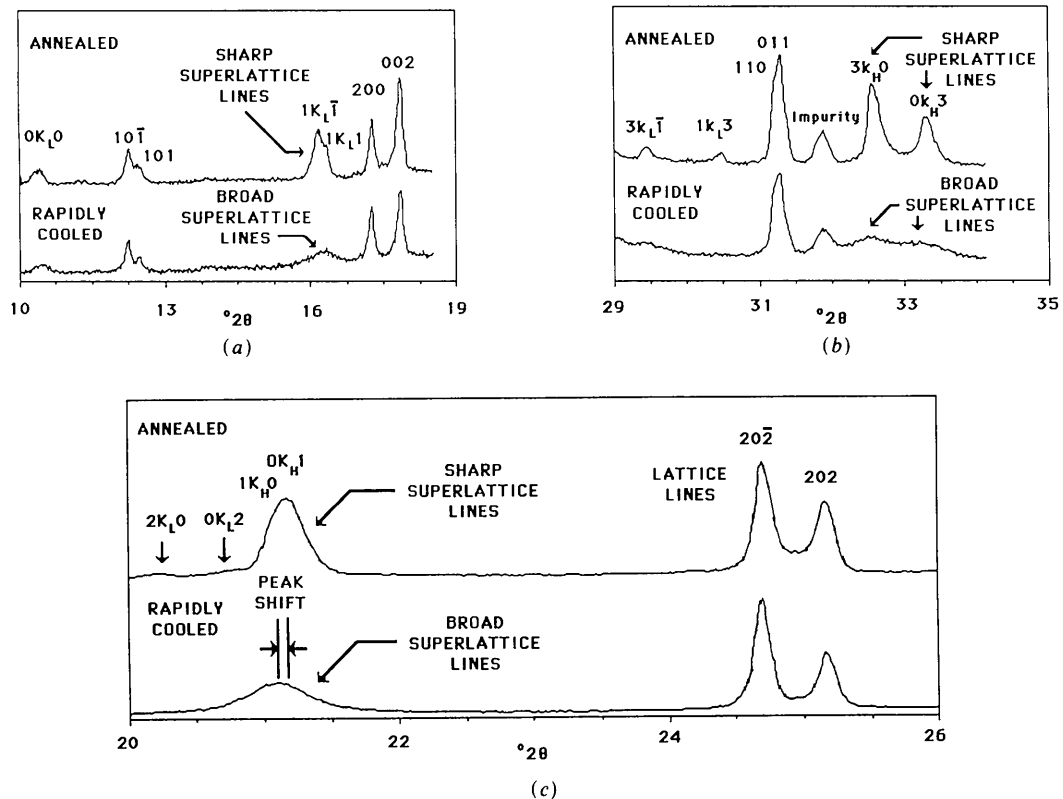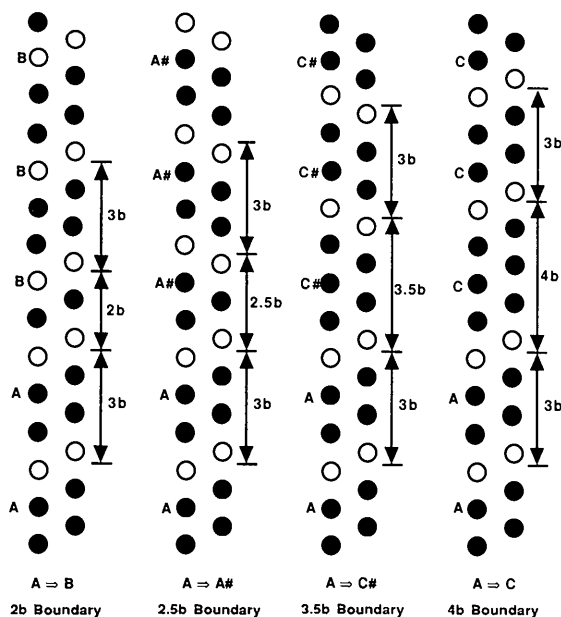

Fig. 2. X-ray powder diffraction patterns from $Ba_xMg_xTi_{8-x}O_{16}$ with $x \simeq 1\cdot33$ using Cu $K\alpha$ radiation showing the superlattice lines between $2\theta = 10$ and $35°$. In the upper pattern in each case the specimen was cooled rapidly from 1230 K and the superlattice lines are broadened due to the formation of antiphase domains. In the lower pattern, the same specimen was subsequently annealed at 1060 K for 160 h to produce well resolved superlattice lines. (c) is expanded in the 2θ direction to show that annealing also produces a shift in the 2θ values of the superlattice lines, but no change in either the 2θ position or the breadth of the lattice lines.
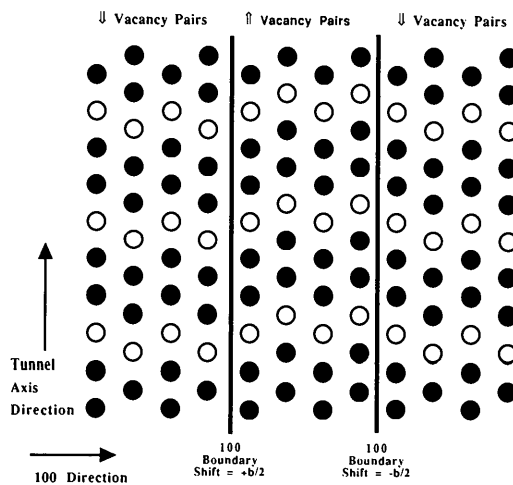
are separated by $3b$, but at the boundary the separation can be $2b$, $2 \cdot 5b$, $3 \cdot 5b$ or $4b$ depending on the cell types in the particular neighbouring domains. All the examples shown are single-layer boundaries. The problem with single-layer boundaries is that certain combinations of domain types cannot exist together without violating the constraint on nearest-neighbour vacancies. By having double-layer or multilayer boundaries all possible types of adjacent domains can coexist. Starting from an A-type domain, a $2b+2b$ boundary layer produces an $A \Rightarrow C$ change whereas a $2b+2 \cdot 5b$ results in an $A \Rightarrow B\#$ change. In some instances a double-layer boundary may be energetically more favourable than a single layer. In particular, the fact that very few Ba hollandites form with more than $1 \cdot 33$ Ba/cell would suggest that three or more consecutive Ba ions along a tunnel are unstable. The boundaries at which this occurs, namely the $3 \cdot 5b$ and $4b$ types, will therefore be the least stable of the four possible types, and combinations based on $2b$ and $2 \cdot 5b$ boundary types will be preferred.

Until now we have only described domain boundaries that form parallel to the (010) plane. Fanchon et al. (1987) have also described boundaries that form perpendicular to the (010) planes. At these boundaries a changeover occurs from ⇓ to ⇑ vacancy pairs or vice versa and the structure is shifted by $+b/2$ or $-b/2$ without the lateral continuity of the vacancy pairing in adjacent tunnels being broken. This is illustrated in Fig. 4(b) for a section of the structure perpendicular to the (010) plane. Although boundaries with shifts other than $\pm b/2$ are possible, Fanchon et al have discounted them either because vacancies occur as nearest neighbours or three adjacent Ba ions exist in a line within the same tunnel. As these boundaries are perpendicular to the (010) plane they have no direct effect on the k index of superlattice peaks. Also, as there is no change in the spacing at a boundary, there is no shift in the h or l index. The

presence of these boundaries, however, will broaden the superlattice spots perpendicular to the b^* direction. Electron micrographs of these boundaries in $Ba_{1.20}(MgTi)_8O_{16}$ do not show any strong planar habit and the boundaries are probably defined by a mixture of (100)/(001) and/or (101)/(10$\bar{1}$) planes. When making general reference to boundaries on planes perpendicular to the (010) plane we will refer to them as ($H0L$) boundaries.

Fig. 4. (a) Single-layer domain boundaries on (010) planes for the changeover from an A-type supercell domain to either a B-, C-, $A\#$- or $C\#$-type supercell domain. In general, the spacing at the boundary is Δb where Δ can be 2, 2·5, 3·5 or 4; (b) domain boundaries on (100) planes defined by a shift in the structure of $\pm b/2$.
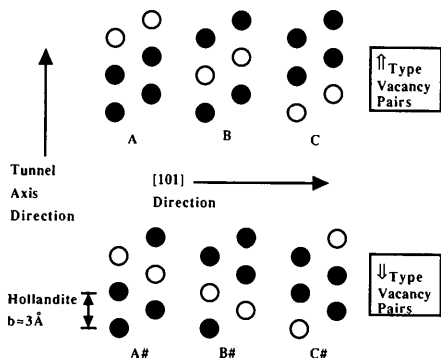

Fig. 3. The six types of supercell in $Ba_{1.33}Mg_{1.33}Ti_{6.67}O_{16}$. In A-, B- and C-type supercells the vacancy pairs are in positions 0,0,0 and $\frac{1}{2},\frac{1}{2},\frac{1}{2}$, (⇑ type). In $A\#$, $B\#$ and $C\#$ supercells the vacancy pairs are in positions 0,0,0 and $\frac{1}{2},-\frac{1}{2},\frac{1}{2}$, (⇓ type).

Derivation of intensity equations

In fully ordered and partially ordered $Ba_{1\cdot33}Mg_{1\cdot33}Ti_{6\cdot67}O_{16}$ the vacancy layers in the (010) planes are always separated by one or more Ba layers. Because of this it is easier to calculate intensities of the superlattice lines from the complementary structure rather than the direct structure (*i.e.* the Ba ions in the hollandite structure are replaced by vacancies and the vacancies by Ba ions). According to Babinet's principle, the intensity pattern of the superlattice lines calculated in this way is identical to the pattern from the structure itself. Two forms of unit cell exist in the complementary structure; one with the $\Downarrow$ configuration of Ba pairs corresponding to $\Downarrow$ pairs of vacancies in the direct structure and the other with the $\Uparrow$ configuration of Ba pairs. For convenience, the origin in each case is shifted to the mid-point between the Ba ions giving atomic positions $\frac{1}{4},\frac{1}{4},\frac{1}{4}$ and $-\frac{1}{4},-\frac{1}{4},-\frac{1}{4}$ for a $\Uparrow$ pair and $\frac{1}{4},-\frac{1}{4},\frac{1}{4}$ and $-\frac{1}{4},\frac{1}{4},-\frac{1}{4}$ for a $\Downarrow$ pair. The structure factors of these cells, assuming integral values for h and l and a continuously varying k, are

$$F_{\Uparrow} = F_{\Downarrow} = (-1)^{h+l}2f\cos\left[(\pi/2)k\right]$$

$$\text{for } h+l = \text{even} \quad (2a)$$

$$F_{\Uparrow} = -F_{\Downarrow} = (-1)^{h+l}2f\sin\left[(\pi/2)k\right]$$

$$\text{for } h+l = \text{odd}. \quad (2b)$$

In the later intensity calculations these structure factors are expressed in general terms as $F = |F|\exp(j\varphi)$ where the phase $\varphi = 0$ or π depending on $h+l$ and the type of pairing. This result implies that a domain structure *without* a boundary layer will produce broadened superlattice reflections only when $h+l$ is odd. For this condition the structure factors in adjacent domains differ in phase by 180° as in Cu_3Au. With reflections having $h+l = $ even, the structure factors in all domains are the same. The fact that all X-ray superlattice lines in hollandites are broadened, not just lines with $h+l = $ odd, indicates that a phase change must also occur in reflections with $h+l$ even. For (010) boundaries this arises from a boundary layer with a spacing other than $3b_{hol}$. Across $(H0L)$ boundaries the phase change at the boundary arises from a shift in the structure of $\pm b/2$ and whether or not there is a phase change 0 or π in the structure factors on either side of the boundary. The problem here is to develop a diffraction theory which accommodates a variable spacing between domains, a phase change in the structure factor and a different boundary model across (010) compared with $(H0L)$ planes. The mathematical technique adopted here follows the general approach of Lifschitz (1937) which has been adapted to the conventional antiphase domain problem by Cheary & Grimes (1972). In this, the amplitude scattered by a crystal with ordered domains is calculated as the sum of the contributions from all the domains before conversion to an intensity. To illustrate how the different boundary models affect the intensity distribution, the calculations are carried out in three parts: (a) the calculation of $I(k)$ at fixed h and l to demonstrate the effect of (010) boundaries alone; (b) the calculation of $I(h)$ and $I(l)$ at fixed k to demonstrate the effects of $(H0L)$ boundaries; (c) the calculation of the intensity function $I(q)$ across an hkl diffraction spot in the direction of the reciprocal-lattice vector $\mathbf{d}^* = h\mathbf{a}^* + k\mathbf{b}^* + l\mathbf{c}^*$, where $q = (2\sin\theta)/\lambda - 1/d$, to demonstrate how all three boundary types can be incorporated into the calculation. The intensity function $I(k)$ is used to interpret the shift of the superlattice lines in electron diffraction patterns. The intensity function $I(q)$ is used to interpret the shifts and the broadening in the powder diffraction profiles and identify the proportions of each boundary type and the (HKL) planes they form on.

(a) Calculation of $I(k)$

Consider a crystal with $M+1$ domains, numbered 0 to M, and let the ith domain have R_i+1 vacancy layers at integral coordinates in the b direction N_i, N_i+3, $N_i+6,\ldots$ up to N_i+3R_i (see Fig. 5a) where N_i corresponds to the position of the first vacancy layer with respect to an origin. The thickness of this domain is $3R_ib$ in the b direction. The amplitude $A_i(k)$ scattered by the ith domain as a function of a continuously variable Miller index k, at particular integral values for h and l, can be expressed as a geometric sum given by

$$A_i(k) = |F|\exp(j\varphi_i)\sum_{r=0}^{R_i}\exp\left[2\pi j(N_i+3r)k\right]$$

$$= |F|\exp(j\varphi_i)\exp\{2\pi jN_ik\}$$

$$\times\{1-\exp\left[6\pi j(R_i+1)k\right]\}$$

$$\times[1-\exp(6\pi jk)]^{-1} \quad (3)$$

where $|F|\exp(j\varphi_i)$ is the structure factor for the ith domain. When $h+l$ is even, φ_i is the same in all domains and has the value 0 or π depending on the value of k [see (2)]. When $h+l$ is odd, φ_i will also be 0 or π depending on the value k, but if domains with $\Uparrow$-type vacancy pairs have $\varphi_i = \pi$ then domains with $\Downarrow$-type vacancy pairs will have $\varphi_i = 0$. Conversely, when $\varphi_i = 0$ for the $\Uparrow$ type then $\varphi_i = \pi$ for the $\Downarrow$ type. Summed over a whole column of $M+1$ domains in the b^* direction the total amplitude $A(k)$ scattered by the crystal is

$$A(k) = \sum_{i=0}^{M}|F|\exp(j\varphi_i)$$

$$\times\exp(2\pi jN_ik)\{1-\exp\left[6\pi j(R_i+1)k\right]\}$$

$$\times[1-\exp(6\pi jk)]^{-1}. \quad (4)$$

The intensity function $I(k)$ for this column of domains will be

$$I(k) = A(k)A^*(k)$$

$$= |F|^2 \sum_{i=0}^{M} \sum_{n=0}^{M} \exp[-j(\varphi_n - \varphi_i)]$$

$$\times \exp[-2\pi j(N_n - N_i)k]$$

$$\times \{1 - \exp[6\pi j(R_i + 1)k]\}$$

$$\times \{1 - \exp[-6\pi j(R_n + 1)k]\}$$

$$\times \{[1 - \exp(6\pi jk)][1 - \exp(-6\pi jk)]\}^{-1}. \quad (5)$$

By implementing the substitutions $n = p + r$ and $i = p$ the intensity can be expressed as the sum of three terms:

$$I(k) = \kappa(I_0 + I_1 + I_1^*) \quad (6)$$

where

$$\kappa = |F|^2\{[1 - \exp(6\pi jk)][1 - \exp(-6\pi jk)]\}^{-1}$$

$$I_0 = \sum_{p=0}^{M} \{1 - \exp[-6\pi j(R_p + 1)k]\}$$

$$\times \{1 - \exp[6\pi j(R_p + 1)k]\}$$

and

$$I_1 = \sum_{r=1}^{M} \sum_{p=0}^{M-r} \exp[-j(\varphi_{p+r} - \varphi_p)]$$

$$\times \exp[-2\pi j(N_{p+r} - N_p)k]$$

$$\times \{1 - \exp[-6\pi j(R_{p+r} + 1)k]\}$$

$$\times \{1 - \exp[6\pi j(R_p + 1)k]\}.$$

The position N_p of the first vacancy layer in the pth domain can be expressed as a recurrence relation,

$$N_p = N_{p-1} + \Delta_{p-1} + 3R_{p-1}$$

$$= \sum_{i=0}^{p-1} \Delta_i + \sum_{i=0}^{p-1} 3R_i \quad (7)$$

where Δ_i is the spacing between the ith and $(i+1)$th domains. Consequently, the differences $N_{p+r} - N_p$ and $\varphi_{p+r} - \varphi_p$ can be expressed as

$$N_{p+r} - N_p = \sum_{i=p}^{p+r-1} \Delta_i + \sum_{i=p}^{p+r-1} 3R_i$$

and

$$\varphi_{p+r} - \varphi_p = \sum_{i=p}^{p+r-1} \Delta\varphi_i$$

where $\Delta\varphi_i$ is the phase difference between the structure factor of the ith and $(i+1)$th domains. When the term $N_{p+r} - N_p$ is substituted back into (6), $I(k)$ can be expressed in terms of averages related to

domain size distribution and the distribution of phase changes at the domain boundaries. For the model developed here we define two terms D and S representing these averages over the crystal,

$$D = \langle \exp[-6\pi jk(R+1)] \rangle \quad \text{and} \quad S = \langle \exp(-j\zeta) \rangle$$

$$(8)$$

where $\zeta = 2\pi k(\Delta - 3) + \Delta\varphi$ = phase change between the end of one domain and the start of the next domain. To include D and S in the calculations and
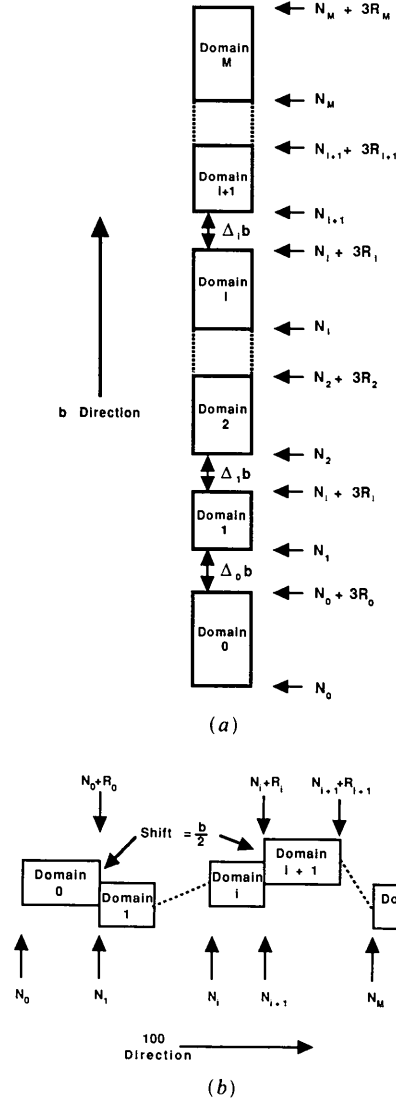

(a)

(b)

Fig. 5. (a) A column of domains in the b direction showing the y coordinates of the first and last vacancy layers in a domain. In the ith domain the first vacancy pair is at $y = N_i b$ and the last one at $(N_i + 3R_i)b$, where $R_i + 1$ is the number of vacancy layers in the ith domain. The spacing of the vacancy pairs at the boundary between the ith and $(i+1)$th domains is $\Delta_i b$. (b) A row of domains in the a direction. In the ith domain there are $R_i + 1$ vacancy pairs between coordinates $x = N_i a$ and $x = (N_i + R_i)a$.

reduce the intensity equation to a manageable form we need to make a number of assumptions:

(i) the crystals are large and incorporate a large number of domains;

(ii) there is no correlation between sizes of adjacent domains so that

$$\left\langle \exp\left[-6\pi jk \sum_{i=1}^{r}(R_i+1)\right]\right\rangle = D^r;$$

(iii) there is no correlation between types of boundary layer in adjacent boundaries so that

$$\left\langle \exp\left(-j\sum_{i=1}^{r}\zeta_i\right)\right\rangle = S^r;$$

(iv) there is no correlation between the boundary type and the domain size.

With these assumptions I_0 and I_1 can be expressed in terms of S and D,

$$\kappa I_0 = [(M+1)|F|^2/4\sin^2 3\pi k][(1-D)+(1-D^*)]$$

and

$$\kappa I_1 = (|F|^2/4\sin^2 3\pi k)\sum_{r=1}^{M}(M+1-r)S^r$$
$$\times[2D^r - D^{r-1} - D^{r+1}].$$

If the antiphase domains are small in relation to the crystal size then D^r will decrease to 0 rapidly with r and $D^M = 0$. Over the range of r for which D^r is significant, $(M+1-r)$ will be more or less constant at $M+1$. Each summation then becomes a geometric progression in which the terms in $D^M = 0$. With large crystals we can also make the substitution $M \simeq M+1$ and (6) reduces to the relatively simple equation

$$I(k) = (M|F|^2/4\sin^2 3\pi k)$$
$$\times[(1-D)(1-S)/(1-SD)$$
$$+(1-D^*)(1-S^*)/(1-S^*D^*)]. \qquad (9)$$

To take this equation further we need to consider the relationship between D and the probability of different size domains P_R where R is the number of layers in a domain in addition to the zeroth layer. The model used here to determine the form of P_R is similar to that developed by Lifschitz (1937). We have assumed that in going from the ith to the $(i+1)$th vacancy layer the probability of the spacing being different from $3b$ is a constant α_b which is independent of position. Given that a spacing other than $3b$ defines a domain boundary, the probability P_R of R layers in a domain in addition to the zeroth layer is given by

$$P_R = \alpha_b(1-\alpha_b)^R, \qquad R \geq 0. \qquad (10)$$

The average domain size T_{010} in the tunnel direction, in terms of the mean number of layers $\langle R \rangle$ in a domain

and the mean number of layers $\langle \Delta \rangle$ at the boundaries, will be

$$T_{010} = b(3\langle R \rangle + \langle \Delta \rangle)$$
$$= 3b[(1-\alpha_b)/\alpha_b + \langle \Delta \rangle/3] \simeq 3b/\alpha_b \qquad (11)$$

assuming $\langle \Delta \rangle$ is close to three hollandite layers. On this basis, D and the intensity equation $I(k)$ along the k direction are given by

$$D = \alpha_b \sum_{R=0}^{\infty}(1-\alpha_b)^R \exp[-6\pi j(R+1)k]$$
$$= \frac{\alpha_b \exp(-6\pi jk)}{[1-(1-\alpha_b)\exp(-6\pi jk)]} \qquad (12)$$

$$I(k) = (M|F|^2/4\sin^2 3\pi k)$$
$$\times[[1-\exp(-6\pi jk)](1-S)$$
$$\times\{[1-\exp(-6\pi jk)]$$
$$+\alpha_b \exp(-6\pi jk)(1-S)\}^{-1}$$
$$+[1-\exp(+6\pi jk)](1-S^*)$$
$$\times\{[1-\exp(+6\pi jk)]$$
$$+\alpha_b \exp(+6\pi jk)(1-S^*)\}^{-1}]. \qquad (13)$$

Further simplification of (13) can be achieved by redefining some of the terms, namely by putting $\psi_b = 1-S$ and $\chi_b = 1-\exp(-6\pi jk)$ to give $I(k)$ as

$$I(k) = M|F|^2(\psi_b + \psi_b^* - \alpha_b\psi_b\psi_b^*)$$
$$\times[4\sin^2 3\pi k - \alpha_b(\chi_b^*\psi_b^* + \chi_b\psi_b) + \alpha_b^2\psi_b\psi_b^*]^{-1}. \qquad (14)$$

To convert this equation into an actual intensity distribution we need to know the form of S, but to do this we need a model to describe the boundary layer between domains. In general, four types of boundary are possible corresponding to a spacing $\Delta = 2, 2\cdot5$, $3\cdot5$ or 4 layers so that with the assumption that the proportion of each type of boundary throughout a crystal is $f_2, f_{2\cdot5}, f_{3\cdot5}$ and f_4 and that $\sum f_i = 1$, then S is given by

$$S = f_2 \exp(2\pi jk) + (-1)^{h+1}f_{2\cdot5}\exp(\pi jk)$$
$$+(-1)^{h+1}f_{3\cdot5}\exp(-\pi jk)$$
$$+f_4 \exp(-2\pi jk). \qquad (15)$$

The $(-1)^{h+1}$ terms in (15) arise because at boundaries with $\Delta = 2\cdot5$ or $3\cdot5$ the vacancies change from $\Uparrow$ pairs to $\Downarrow$ pairs (or vice versa) which for lines with $(h+1) =$ odd corresponds to a change from F to $-F$ (or vice versa) and $\zeta = +\pi$ or $-\pi$.

(b) Calculation of $I(h)$ [or $I(l)$]

To calculate the intensity distribution $I(h)$ of the superlattice lines as a function of h we need to consider a line of cells consisting of vacancy pairs along the a direction as shown in Fig. 5(b). In this model

as in the earlier model there are $M+1$ domains numbered 0 to M and in the ith domain the vacancy pairs have x coordinate from N_i to $N_i + R_i$ where $R_i + 1$ is the number of vacancy pairs in the ith domain. A domain boundary is defined by a shift in the b direction of $y = \frac{1}{2}$ or $-\frac{1}{2}$, but there is no change in the spacing at the boundary. The phase difference ζ between structure factors either side of a boundary arises from two effects:

(a) the changeover from $\Uparrow$ to $\Downarrow$ vacancy pairs (or vice versa) which gives $\zeta = \pm\pi$ for $h+l = $ odd and $\zeta = 0$ for all other reflections and

(b) the shift in origin of $y = \pm\frac{1}{2}$ which adds a further $\pm\pi k$ to ζ.

For this problem the intensity distribution can be derived in exactly the same way as $I(k)$ earlier but summing along the a or c directions in steps of 1 unit cell at a time. Under this condition, $I(h)$ will be given by

$$I(h) = (M|F|^2/4\sin^2 \pi h)[(1-D)(1-S)/(1-SD)$$
$$+ (1-D^*)(1-S^*)/(1-S^*D^*)] \qquad (16)$$

where $D = \langle \exp[-2\pi j(R+1)h] \rangle$ and $S = \langle \exp(-j\zeta) \rangle = \frac{1}{2}(-1)^{h+1}[\exp(j\pi k) + \exp(-j\pi k)]$. With the assumption that the probability of an $(H0L)$ boundary occurring between any two vacancy pairs is α_a and the probability P_R of R pairs in addition to the zeroth pair is $P_R = \alpha_a(1-\alpha_a)^R$ then the mean domain size in the [100] direction $T_a = a\langle R+1 \rangle = a/\alpha_a$. The simplified equation for the superlattice lines (and not the lattice lines) in which $\psi_a = 1-S$ and $\chi_a = 1 - \exp(-2\pi jh)$ is

$$I(h) = M|F|^2(\psi_a + \psi_a^* - \alpha_a\psi_a\psi_a^*)$$
$$\times [4\sin^2 \pi h - \alpha_a(\chi_a^*\psi_a^* + \chi_a\psi_a) + \alpha_a^2\psi_a\psi_a^*]^{-1}. \qquad (17)$$

Based on the phase changes given above, the term ψ_a for these boundaries is real and given by $\psi_a = \psi_a^* = [1-(-1)^{h+1}\cos \pi k]$. Also, close to the centre of the superlattice line, h can be put as $h = n + \varepsilon_h$, where n is an integer, and $\sin^2 \pi h \simeq (\pi\varepsilon_h)^2$. By incorporation of these results into (17), the intensity distribution $I(\varepsilon_h)$ becomes Lorentzian centred on an integral value for h,

$$I(\varepsilon_h) = M|F|^2\psi_a(2-\alpha_a\psi_a)$$
$$\times [(1-\alpha_a\psi_a)(2\pi\varepsilon_h)^2 + \alpha_a^2\psi_a^2]^{-1}. \qquad (18)$$

In this instance there is no shift in the peak value off the $h = $ integer condition, but the profile is symmetrically broadened. In an X-ray powder pattern only those lines with $k \simeq 2/3$ and $h+l = $ odd number or $k \simeq 1/3$ and $h+l = $ even number are intense enough to be detected. In each of these cases $\psi_a = 1/2$ and the full width at half-maximum intensity δ_h (or apparent particle size T_{app}) is given by

$$\delta_h = T_{app}^{-1} \simeq \alpha_a/2\pi(1-\alpha_a/2)^{1/2}. \qquad (19)$$

(c) *Calculation of $I(q)$*

The intensity distribution across the hkl powder diffraction line is given by considering the average intensity scattered by the column of vacancy pairs (or cells) perpendicular to the (hkl) plane. By adding up the amplitude from each domain in this column in the same way as in the previous derivations, an intensity equation $I(Q)$ analogous to (14) and (17) can be formulated but expressed this time in terms of the scattering vector Q [$= 2(\sin \theta)/\lambda$] and the d spacing of the (hkl) plane,

$$I(Q) = M|F|^2(\psi_d + \psi_d^* - \alpha_d\psi_d\psi_d^*)$$
$$\times [4\sin^2 \pi Qd - \alpha_d(\chi_d^*\psi_d^* + \chi_d\psi_d) + \alpha_d^2\psi_d\psi_d^*]^{-1}$$
$$\qquad (20)$$

where $\chi_d = 1 - \exp(-2\pi jQd)$. The mean domain thickness in this direction $T_d = d/\alpha_d$, where α_d is the probability of a domain boundary between adjacent cells. The term $\psi_d = 1-S$ where $S = \exp(-j\zeta)$ and ζ is the phase change at a domain boundary which could be any one of the two possible types [$i.e.$ (010) or ($H0L$)]. It is worth remarking that $I(Q)$ can be converted to $I(k)$ by putting $Q = k/b$ and $d = 3b$ or to $I(h)$ by putting $Q = h/a$ and $d = a$.

The intensity distribution about an individual peak can be developed by putting $Q = q + 1/d$ and dividing ψ_d into its real and imaginary parts, $\psi_d = \psi_r + j\psi_i$. In the vicinity of the peak maximum where q is small $\sin \pi qd \simeq \pi qd$ and the intensity function $I(q)$ will be given by

$$I(q) = M|F|^2[2\psi_r - \alpha_d(\psi_r^2 + \psi_i^2)]$$
$$\times [(2\pi qd)^2(1-\alpha_d\psi_r)$$
$$+ 4\pi q\, d\alpha_d\psi_i + \alpha_d^2(\psi_r^2 + \psi_i^2)]^{-1}. \qquad (21)$$

Further, on the assumption that ψ_r and ψ_i are more or less constant across a profile, $I(q)$ can also be expressed as a Lorentzian,

$$I(q) = A_q/[(q - q_0)^2 + (\delta/2)^2] \qquad (22)$$

in which q_0, the shift from the ideal $3b$ hollandite superstructure in $1/d$ units, and δ, the full width at half-maximum intensity in $1/d$ units, are given by

$$q_0 = -\psi_i\alpha_d/2\pi d(1-\alpha_d\psi_r)$$

and

$$\delta^2 = 1/T_{app}^2 = (\psi_r\alpha_d)^2/(\pi d)^2(1-\alpha_d\psi_r) - \psi_r\alpha_d(2q_0)^2. \qquad (23)$$

It should be noted that the shift of the diffraction peak q_0 is given by the value of ε_0, the shift in the [010] direction, resolved in the direction of d^* and converted to $1/d$ units. Further consideration will be given to the behaviour of $I(q)$ later when analysing the powder diffraction data.

Table 1. *A comparison of the observed and calculated shifts ε_0 of the superlattice peaks relative to the hollandite lattice indices $k = 1/3$ and $k = 2/3$ for the antiphase domains with boundary spacings $\Delta = 2, 2\cdot5, 3\cdot5$ and 4 layers*

The calculated values are based on equation (20) with $\alpha_b = 0\cdot2$ (*i.e.* mean domain size $\simeq 45$ Å).

		$h + l$ = even			$h + l$ = odd		
		ε_0 $(k \simeq 1/3)$	ε_0 $(k \simeq 2/3)$	$\dfrac{I(k \simeq 1/3)}{I(k \simeq 2/3)}$	ε_0 $(k \simeq 1/3)$	ε_0 $(k \simeq 2/3)$	$\dfrac{I(k \simeq 1/3)}{I(k \simeq 2/3)}$
Observed:		+0·01	~+0·01	≫1	~−0·01	~−0·01	≪1
Calculation							
Δ	ρ						
2	-2π	0·012	−0·013	2·7	0·012	−0·013	2·7
2·5	$-\pi$	0·010	0·012	11·4	−0·012	−0·010	0·1
3·5	$+\pi$	−0·010	−0·014	10	0·014	0·010	0·1
4	$+2\pi$	−0·014	−0·013	3·3	−0·014	−0·013	3·3

Analysis of experimental data

1. *Interpretation of electron diffraction results*

The experimental electron diffraction data for $Ba_{1\cdot33}Mg_{1\cdot33}Ti_{6\cdot67}O_{16}$ (Bursill & Grzinic, 1980) may be summarized as follows:

(*a*) superlattice peaks occur at $k = 1/3 + \varepsilon_0$ and $2/3 + \varepsilon_0$ where $\varepsilon_0 = 0\cdot006$ to $0\cdot012$ for $h + l$ = even and $\varepsilon_0 = -0\cdot006$ to $-0\cdot012$ for $h + l$ = odd;

(*b*) for $h + l$ = odd, $I_{max}(k \simeq 2/3) \gg I_{max}(k \simeq 1/3)$ but for $h + l$ = even, $I_{max}(k \simeq 2/3) \ll I_{max}(k \simeq 1/3)$;

(*c*) the mean domain size along the tunnel direction is in the vicinity of 40–50 Å.

To explain this behaviour we need to examine how different boundary models affect the intensity distribution $I(k)$ given by (14). For this function to peak at exactly $k = 1/3$ or $2/3$ the term ψ_b must be real. Alternatively, for the peak to be shifted off this condition, ψ_b must be complex. On this basis a domain structure consisting of equal proportions of all four types of boundary spacings Δ would not produce a shift in the superlattice line as S [defined in (15)] would be real. Despite the large number of possible boundary models based on differing proportions of each boundary spacing, it is possible to explain the essential characteristics of the superlattice peaks in terms of a single boundary type.

When all the (010) domain boundaries have the same spacing, the function S contains one term $S = \gamma \exp(-jpk)$ where $p = 2\pi(\Delta - 3)$. The term $\gamma = 1$ for all models with $h + l$ = even and only becomes -1 when $\Delta = 2\cdot5$ or $3\cdot5$ and $h + l$ = odd. The intensity function $I(k)$,

$$I(k) = 4Mf^2(1 - \alpha_b)(1 - \gamma \cos pk)(1 + \gamma \cos \pi k)$$
$$\times \{4 \sin^2(3\pi k)[1 - \alpha_b(1 - \gamma \cos pk)]$$
$$+ 2\gamma\alpha_b \sin 6\pi k \sin pk + 2\alpha_b^2(1 - \gamma \cos pk)\}^{-1}$$

$$\text{(24)}$$

where f is the atomic scattering factor of Ba. When this function is plotted as a function of k, from 0 to 1, two peaks are evident at $k \simeq 1/3$ and $k \simeq 2/3$. Each model has its own characteristics but only the model

with a boundary spacing $\Delta = 2\cdot5$ (*i.e.* $\rho = -\pi$) accords with the observed characteristics. This is highlighted in Table 1 which compares the observed diffraction behaviour with the relative intensities and shifts of the diffraction peaks calculated from (24) for a mean domain size of ~45 Å (*i.e.* $\alpha_b = 0\cdot2$). The actual peak shifts given by the $\Delta = 2\cdot5$ model agree quantitatively with observations of Bursill & Grzinic (1980) in that a domain size of 45 Å produces a shift in k of $0\cdot01$ (*i.e.* a multiplicity $m = 5\cdot83$). It should be noted, however, that the peak shift at a fixed $h + l$ is marginally different for the weak and strong superlattice lines. An exact relationship between the peak shift and the mean domain size cannot be derived. An approximate equation, however, can be derived by putting k in (24) as $k = k_0 + \varepsilon$ where $k_0 = 1/3$ or $2/3$ and ε is small (*i.e.* $0\cdot02$ or smaller). Under these conditions the small-angle approximation $\sin^2 3\pi k \simeq (3\pi\varepsilon)^2$ may be implemented, and provided $\sin \rho k \simeq \sin \rho k_0$ and $\cos \rho k \simeq \cos \rho k_0$ over a peak, then the profiles are Lorentzian,

$$I(\varepsilon) = A_k/[(\varepsilon - \varepsilon_0)^2 + (\delta/2)^2] \quad \text{(25)}$$

where ε_0 is the shift of the peak maximum relative to $k_0 = 1/3$ or $2/3$ and δ is the full width at half-maximum intensity (FWHM) in Miller index units. For the $\Delta = 2\cdot5$ model the peak shift ε_0 obtained by this approach is accurate to within a few percent for the strong superlattice lines and given by

$$\varepsilon_0 = \frac{(-1)^{h+1}\alpha_b \sin \pi k_0}{6\pi\{1 - \alpha_b[1 - (-1)^{h+1} \cos \pi k_0]\}}. \quad \text{(26)}$$

It should be emphasized that the presence of only $\Delta = 2\cdot5$ boundaries makes sense. In the first place, the only commensurate superstructures in hollandites are those with either a $2\cdot5b$ or a $3b$ spacing between the vacancy layers. On this basis boundaries with $\Delta = 2\cdot5$ will be preferred energetically over other boundary types and the variation in stoichiometry at the boundary will be minimized. Nevertheless, because a $2\cdot5b$ boundary contains one less Ba ion than a $3b$ layer, the total tunnel occupancy of any

hollandite containing antiphase domains will always be less than 67% ($x = 4/3$). For an average domain structure consisting of $5 \times 3b$ supercells and a $2.5b$ boundary layer (*i.e.* an average domain size $\simeq 47$ Å), the occupancy will be $23/35 = 65.71\%$ or $x = 1.314$. This result is reflected in the preparation of samples of $x = 1.33$ hollandites which invariably contain weak second-phase diffraction lines in the X-ray powder pattern which we have not been able to identify.

2. Analysis of powder diffraction data

In the two powder diffraction patterns illustrated in Fig. 2 the superlattice lines are broadened relative to the lattice lines. The superlattice broadening in the annealed sample is less than the quenched sample and there is a difference in the peak positions of the two sets of superlattice lines. Heat treatment has no significant effect on the breadth or position of the lattice lines. The purpose of this section is to use (23) to explain the observed broadening δ of the superlattice lines. In the following analysis it is assumed that boundaries form on (010) and ($H0L$) planes and that all the (010) boundaries consist of a $2.5b$ boundary layer. The function S for an hkl line with a combination of boundaries will depend on the proportion of each type of boundary,

$$S = \langle \exp(j\zeta) \rangle = \Gamma S_{010} + (1-\Gamma)S_{H0L}$$
$$= (-1)^{h+1}[\Gamma \exp(\pi jk) + (1-\Gamma)\cos \pi k] \quad (27)$$

where Γ is the proportion of (010) boundaries along a line perpendicular to the (hkl) plane. $\Gamma = 1$ in the [010] direction as all the boundaries are (010) type but in any perpendicular [$h0k$] direction $\Gamma = 0$ as all the boundaries are ($H0L$) type. In general, ψ_d will be given by

$$\psi_d = 1 - S = \psi_r + j\psi_i$$
$$= [1 - (-1)^{h+1}\cos \pi k] - j\Gamma(-1)^{h+1}\sin \pi k. \quad (28)$$

As the detectable superlattice lines in the powder pattern are all of the type $h + l =$ even and $k \simeq 1/3$ or $h + l =$ odd and $k \simeq 2/3$ then $\psi_r = 1/2$ and $\psi_i = -\Gamma(-1)^{h+1}3^{1/2}/2$. The shift q_0 and the FWHM δ given in (23) become

$$q_0 = \frac{(-1)^{h+l}\Gamma 3^{1/2}\alpha_d}{4\pi d(1 - \alpha_d/2)} \quad (29a)$$

and

$$\delta^2 = \frac{1}{T_{app}^2} = \frac{\alpha_d^2}{(2\pi d)^2(1 - \alpha_d/2)} - 2\alpha_d(q_0)^2 \quad (29b)$$

where d/α_d is the mean domain size perpendicular to the (hkl) plane. For an $0k0$ superlattice line $\Gamma = 1$ and there is no contribution from ($H0L$) boundaries to q_0 or δ. The shift in the k value, ε_0, from the ideal

superlattice value given by (26) and the apparent particle size from (29b) for $0k0$ lines simplify to

$$|\varepsilon_0| = 0.0459\alpha_b/(1 - \alpha_b/2) \quad (30a)$$

and

$$\delta = \frac{1}{T_{app}} = \frac{\alpha_b(1 - 2\alpha_b)^{1/2}}{(2\pi d)(1 - \alpha_b/2)} \quad (30b)$$

where the mean domain size in the [010] direction is given by $3b/\alpha_b$.

Two sets of X-ray powder data have been collected from a single specimen of $Ba_xMg_xTi_{8-x}O_{16}$ ($x \simeq 1.33$) to test the validity of the above equations. The first data set was collected from a freshly prepared specimen with extensively broadened superlattice lines which was cooled from 1230 K to room temperature over a 2 h period. The second data set was collected after annealing the specimen at 1060 K (*i.e.* just below the order–disorder temperature) for 160 h. As indicated earlier in Fig. 2, this heat treatment shifts the superlattice lines, reduces their breadth but does not have any significant effect on the lattice lines. The specimen used in this study was a 25 mm sintered disc prepared by solid-state reaction of TiO_2, MgO and $BaCO_3$ as described in Cheary & Squadrito (1989). In each case the X-ray powder data were collected by step scanning from $2\theta = 10$ to $2\theta = 35°$ with $0.01°$ steps for 70 s step^{-1} on an Apex diffractometer using a Philips long fine-focus X-ray tube with a Cu target ($\lambda = 1.5406$ Å). To use (29) and (30) on the recorded X-ray count data it was necessary to correct the diffraction profiles for instrumental effects, the emission profile and particle size. This was done using a fitting program developed in this laboratory (Cheary & Coelho, 1992) which convolutes a Lorentzian profile with an instrumental profile. The parameters for the instrumental profile of the diffractometer were determined from a reference powder specimen of MgO with a crystallite size of 2 μm by fitting a convolution of analytical profile shapes for axial divergence, flat specimen error, receiving-slit width, target size, specimen tilt and the Cu $K\alpha$ emission profile (Wilson, 1963; Klug & Alexander, 1974). Observation under a JEOL 35C scanning electron microscope indicates that the hollandite specimen used in this work possesses small crystallites ~ 3000 Å and as such the lattice lines are slightly broader than expected. To determine the contribution of the antiphase domains to the broadening of the superlattice lines, it was assumed that the FWHM of the Lorentzian profile convoluted into the instrumental profile arises from particle size only in the lattice lines and particle size + antiphase broadening in the superlattice lines. In the fitting program, the width of the Lorentzian $FWHM_{2\theta}$ is expressed in terms of an apparent particle size T_{app} using the relation $FWHM_{2\theta} = \lambda / T_{app} \cos \theta$ rad. The apparent particle size T_{app}^{dom} in Å arising from antiphase domains alone

Table 2. *The measured peak 2θ values, shifts ε_0 of the k index from the commensurate values and the corrected apparent particle sizes T^{dom}_{app} for the superlattice lines from* $Ba_x(Mg/Ti)$ *hollandite with* $x \simeq 1\cdot33$ *(a) cooled rapidly from* 1230 K *to room temperature and* (b) *after further annealing at* 1060 K *for* 160 h

The lattice parameters obtained for this specimen are $a = 10\cdot249\,(7)$, $b = 2\cdot978\,(2)$, $c = 9\cdot915\,(7)$ Å and $\beta = 91.05\,(2)°$ using $\lambda = 1\cdot5406$ Å.

	(a) Rapidly cooled specimen			(b) Annealed specimen		
$h\,k\,l$	2θ (°)	ε_0	T^{dom}_{app} (Å)	2θ (°)	ε_0	T^{dom}_{app} (Å)
$0\,k_L\,0$	10·506 (10)	0·0207 (3)	478 (60)	10·430 (6)	0·0181 (2)	1110 (130)
$1\,k_L\,1$	16·231 (15)	0·0238 (8)	147 (10)	16·167 (3)	0·0193 (2)	3920 (1200)
$1\,k_L\,\bar{1}$	16·391 (15)	0·0227 (8)		16·326 (3)	0·0192 (2)	
$1\,k_H\,0$	21·078 (6)	−0·0218 (2)	225 (10)	21·146 (3)	−0·0195 (1)	865 (70)
$0\,k_H\,1$	21·210 (6)	−0·0216 (2)		21·280 (5)	−0·0189 (2)	
$3\,k_H\,0$	32·498 (4)	−0·0239 (2)	147 (12)	32·582 (3)	−0·0206 (1)	1310 (140)
$0\,k_H\,3$	33·229 (4)	−0·0245 (2)		33·314 (2)	−0·0197 (1)	

is equivalent to $1/\delta$ in (29) and (30) and for each superlattice line is given by

$$1/T^{dom}_{app} = 1/T^{superlattice}_{app} - 1/T^{lattice}_{app} \qquad (31)$$

where $T^{superlattice}_{app}$ is the apparent particle size of the superlattice line and $T^{lattice}_{app}$ is the apparent particle size of a nearby lattice line.

In the present analysis only the strongest superlattice lines have been analysed. These are the $0k_L0$, the $1k_L\bar{1}/1k_L1$ doublet, the $1k_H0/0k_H1$ doublet and the $3k_H0/0k_H3$ doublet where $k_L \simeq 1/3$ and $k_H \simeq 2/3$. In the annealed specimen the doublets can be resolved into two lines but in the rapidly cooled specimen these lines are very broad and cannot be resolved. In the evaluation of the profile parameters various constraints were incorporated in the fitting procedure to ensure that the results were physically realistic:

(i) the relative integrated intensities of all the peaks are the same in each data set;

(ii) the 2θ separation of the peaks in the superlattice doublets are the same in the annealed and freshly prepared specimens;

(iii) in each superlattice doublet the apparent particle size is the same for each peak;

(iv) the apparent particle size of the same lattice lines in each data set are the same.

The results of this fitting are summarized in Table 2 which gives the peak 2θ values of the superlattice lines along with the corrected apparent particle sizes T^{dom}_{app} arising from antiphase domains and the shift ε_0 of the k index of these lines from their ideal values (*i.e.* 1/3 or 2/3). The ε_0 values were obtained by examining the difference in $1/d^2$ values between each superlattice line and a nearby lattice line in order to minimize errors arising from specimen surface displacement and zero error. In this way it is not necessary to know any of the monoclinic lattice parameters other than b. For example, with the $1k_L1$ line, $\varepsilon_0 = k_L - 1/3$ and k_L was determined using the relation

$$k_L^2/b^2 = 1/d^2_{1k_L1} - 1/d^2_{101}. \qquad (32)$$

Even after many days of annealing just below the order–disorder temperature, the superlattice lines still display some diffraction broadening relative to the lattice lines. This indicates that domains of some form still exist within the annealed sample. In both sets of results in Table 2 the superlattice lines are shifted from $k = 1/3$ or $2/3$ and the magnitude of this shift is relatively uniform for the lines that are readily detected. As expected both the shift and the breadth of the superlattice lines are greater for the rapidly cooled specimen and on annealing the 2θ value of lines with $k \simeq 1/3$ decreases whilst the 2θ value of lines with $k \simeq 2/3$ increases. The magnitude of the movement induced by annealing is typically between $0\cdot06$ and $0\cdot08°2\theta$. When averaged over all the lines in Table 2 the change in $|\varepsilon_0|$ induced by annealing is $\sim 0\cdot004\,(1)$.

One check on the diffraction theory developed here is to compare the observed change in $|\varepsilon_0|$ on annealing with the change calculated through (30a). To do this it is necessary to determine the α_b values for the annealed and rapidly cooled specimens. For all the superlattice lines except the $0k_L0$ line, the relationship between T^{dom}_{app} and α_b is complicated and dependent on the proportion of $(H0L)$ boundaries accompanying (010) boundaries. The breadth of the $0k_L0$ line is only affected by (010) boundaries as the $(0k_L0)$ plane is perpendicular to all the $(H0L)$ boundary planes. The value of α_b can therefore be determined directly from T^{dom}_{app} through (30b). Accordingly, the values of α_b for the rapidly cooled and annealed specimens are $0\cdot127\,(19)$ and $0\cdot052\,(7)$, respectively. The corresponding values of $|\varepsilon_0|$ calculated from (30a) using these α_b values are $0\cdot0062$ and $0\cdot0025$. The change in $|\varepsilon_0|$ calculated in this way is $0\cdot0037$ which agrees well with the observed value of $0\cdot004(1)$.

Although the observed and calculated changes in $|\varepsilon_0|$ agree well, there is a large discrepancy between the absolute theoretical and observed values for $|\varepsilon_0|$. For the rapidly cooled specimen the average $|\varepsilon_0|$ is $\sim 0\cdot023$, which is significantly larger than the calculated value of $0\cdot006$. Even for the annealed specimen the observed $|\varepsilon_0|$ is still $\sim 0\cdot019$. The extent to which the observed $|\varepsilon_0|$ values change with the line breadth or $1/T^{dom}_{app}$ suggests that $|\varepsilon_0|$ will still be $\sim 0\cdot016$ in the

Table 3. *The shifts q_0 and $|\varepsilon_0^*|$ for the superlattice lines from the rapidly cooled and annealed specimens along with the mean domain size T_d perpendicular to the diffracting plane*

The shift terms are measured relative to the reference 2θ position for each line at which the diffraction line broadening arising from domains appears to be zero.

	(a) Rapidly cooled specimen			(b) Annealed specimen		
	$q_0 \times 10^4$ (Å^{-1})	$|\varepsilon_0^*|$	$T_d = d/\alpha_d$ (Å)	$q_0 \times 10^4$ (Å^{-1})	$|\varepsilon_0^*|$	$T_d = d/\alpha_d$ (Å)
$0\,k_L\,0$	15·2	0·0048	54 (7)	6·7	0·0021	123 (15)
$1\,k_L\,1$ $1\,k_L\,\bar{1}$	7·6	0·0037	25 (2)	0·4	0·0002	610 (190)
$1\,k_H\,0$ $0\,k_H\,1$	10·4	0·0033	34 (2)	2·7	0·0008	132 (10)
$3\,k_H\,0$ $0\,k_H\,3$	10·3	0·0049	24 (2)	1·2	0·0006	203 (22)

absence of line broadening (*i.e.* when $1/T_{app}^{dom} = 0$). On the basis of the antiphase domain model presented here an ideal specimen of fully ordered $Ba_{1.33}Mg_{1.33}Ti_{6.67}O_{16}$ would give $|\varepsilon_0| = 0$. Consequently, the absolute shift $|\varepsilon_0|$ of the observed super-lattice lines cannot be accounted for by antiphase domains alone; other factors must play a part and in this instance the most likely cause is the formation of an intergrowth of $3b$ domains with a small proportion of $5b$ domains (Bursill & Grzinic, 1980). According to the intergrowth model of Mijlhoff *et al.* (1985) reflected by (1), the minimum $|\varepsilon_0| \simeq 0.016$ corresponds to a composition of $\sim 1.30\,\text{Ba/cell}$ rather than $1.33\,\text{Ba/cell}$. The presence of $5b$ domains in addition to $3b$ domains casts some doubt on the validity of using the present theory on the current powder data. We contend, however, that as most of the domains in the specimen are probably $3b$ domains the theory will still be good enough to obtain reasonable absolute estimates of the mean domain sizes T_d in the various d_{hkl}^* directions. More importantly, the relative domain sizes in the d_{hkl}^* directions can still be used to identify the $(H0L)$ planes forming the boundaries. Further justification for continuing with the implementation of the present theory is given by the fact that it is consistent when applied to changes in $|\varepsilon_0|$ and that the broadening contribution of $(H0L)$ boundaries is the same irrespective of whether they are in a $5b$ region or a $3b$ region. Nevertheless, we are currently working on how the diffraction theory can be generalized to a model with inter-growths of $3b$ and $5b$ regions (and $5b$ and $2b$ regions) with antiphase domains included in each region to explain the broadening across the complete solid-solution range from $Ba_{1.14}Mg_{1.14}Ti_{6.86}O_{16}$ to $Ba_{1.33}Mg_{1.33}Ti_{6.67}O_{16}$.

To obtain an accurate mean domain size $T_d (=d/\alpha_d)$ from each value for T_{app}^{dom} in Table 2 using (29b), it is also necessary to know the appropriate value for the shift q_0 for each superlattice line. We have made the assumption that the appropriate value for q_0 is not the absolute shift relative to the 2θ

corresponding to $k = 1/3$ or $2/3$, but is the shift relative to the 2θ value for which $1/T_{app} = 0$ (*i.e.* $2\theta_{ref}$). In this work we have determined $2\theta_{ref}$ by assuming that the 2θ angle of each superlattice in the annealed and rapidly cooled specimens is given approximately by $2\theta = 2\theta_{ref} + C/T_{app}^{dom}$ where C is a constant for a particular line. The term q_0 is then given by $(2\theta - 2\theta_{ref})\cos\theta/\lambda$. The values of q_0 determined in this way for all the superlattice lines are presented in Table 3 along with the mean domain thickness values T_d obtained from (29b). It should be noted that the shifts q_0 are small and have little effect on the value of T_d obtained as $1/(T_{app}^{dom})^2 \gg 2\alpha_d q_0^2$ and values within 2% of those quoted in Table 3 could have been obtained by writing (29b) as

$$1/T_{app}^{dom} = \frac{\alpha_d}{2\pi d(1-\alpha_d/2)^{1/2}}.$$

Also included in Table 3 are the corresponding shifts $|\varepsilon_0^*|$ in the k index relative to the above reference $2\theta_{ref}$ values and given by $\varepsilon_0^* = b^2 q_0/dk$ where d is the d spacing, b is the lattice parameter and $k = 1/3$ or $2/3$. (Note: the term $\varepsilon_0^* \neq \varepsilon_0$, the latter is the shift relative to $k = 1/3$ or $2/3$.)

To identify the planes on which the domain boundaries form, we have used the method of Wilson & Zsoldos (1965). The algebra involved in applying this method to a monoclinic lattice is unnecessarily complicated. With most monoclinic hollandites $\beta \simeq 90°$ and $a \simeq c$ and very little error is incurred by assuming the unit cell is tetragonal with b as the unique axis and $a_{tet} = [(ac)_{mono}]^{1/2}$. In $Ba_{1.33}Mg_{1.33}Ti_{6.67}O_{16}$, a and c differ by only 3% and $\beta \simeq 91°$. Two boundary models have been examined.

Model A: Boundaries on the (100) and (001) planes with a mean domain size $T_{100} = a_{tet}/\alpha_a$ in each of the corresponding directions and boundaries on the (010) plane with a mean domain size $T_{010} = 3b/\alpha_b$ in the [010] direction.

Model B: Boundaries on the (101) and ($10\bar{1}$) planes with a mean domain size $T_{101} = d_{101}/\alpha_{101}$ in each of the corresponding directions and boundaries on the

(010) plane with a mean domain size $T_{010} = 3b/\alpha_b$ in the [010] direction.

The variation of the mean domain size T_d with hkl for these models is reflected in the two equations below:

model A

$$\frac{1}{T_d d} = \frac{|h| + |l|}{a_{\text{tet}} T_{100}} + \frac{k}{T_{010} b};\qquad (33)$$

model B

$$\frac{1}{T_d d} = \frac{d_{101}(|h+l| + |h-l|)}{a_{\text{tet}}^2 T_{101}} + \frac{k}{T_{010} b}.\qquad (34)$$

These models have been applied to the present data and of the two model B gives the better fit for both the rapidly cooled and annealed specimens. This is illustrated in the plots of b/kdT_d against $bd_{101}(|h + l| + |h + l|)/ka_{\text{tet}}^2$ shown in Fig. 6 which are both reasonably linear. The slope and intercept of the graph for the rapidly cooled specimen indicate a mean domain size T_{101} between (101) boundaries in the [101] direction of 31 (5) Å and a mean domain size T_{010} between (010) boundaries in the [010] direction of 70 (10) Å. The annealed specimen gives a slope $\simeq 0$ and an intercept corresponding to $T_{010} = $ 170 (10) Å. In this specimen very few boundaries form on the (101) or ($10\bar{1}$) planes. Annealing therefore acts on (101) boundaries to a far greater extent than

the (010) boundaries which are more stable and less mobile. A reduction in the number of (010) boundaries can only occur if the boundaries diffuse to the crystal surface or if they coalesce into multilayer boundaries.

Concluding remarks

The theory developed here for interpreting X-ray line profiles in terms of the antiphase domain structure in $Ba_{1.33}Mg_{1.33}Ti_{6.67}O_{16}$ appears to be consistent with the current data. As such it can be used as the basis for investigating the thermodynamics of domain growth in this material. In its present form the diffraction theory is not strictly applicable to hollandites with Ba concentrations other than $x \simeq 1.33$ and further work is required to generalize the present approach to any composition in the solid-solution range. This will allow the thermodynamics of any hollandite domain structure to be investigated by X-ray powder diffraction.
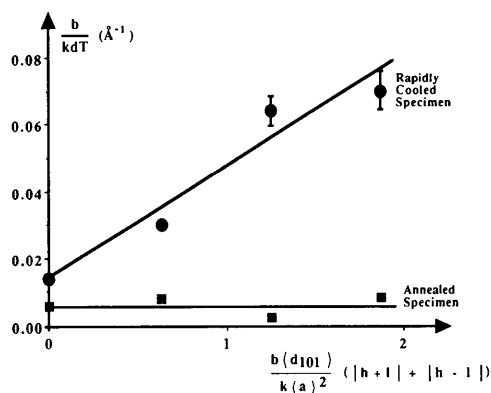
Fig. 6. A plot based on the corrected apparent particle size T from the broadened superlattice lines in the rapidly cooled and annealed samples. The fitted line for the annealed sample has zero slope and only (010) domain boundaries are present with an average domain size of 170 Å. In the rapidly cooled specimen the fitted line suggests domain boundaries on the (101) planes, with an average domain size of 31 (5) Å in the [101] direction and on the (010) plane with an average domain size of 70 (10) Å in the [010] direction.

References

BURSILL, L. A. & GRZINIC, G. (1980). *Acta Cryst.* B36, 2902-2913.
CHEARY, R. W. (1987). *Acta Cryst.* B43, 28-34.
CHEARY, R. W. & COELHO, A. (1992). *J. Appl. Cryst.* In the press.
CHEARY, R. W. & GRIMES, N. W. (1972). *Acta Cryst.* A28, 454-458.
CHEARY, R. W. & SQUADRITO, R. (1989). *Acta Cryst.* B45, 205-212.
FANCHON, E., VICAT, J., HODEAU, J. L., WOLFERS, P., TRAN QUI, D. & STROBEL, P. (1987). *Acta Cryst.* B43, 440-448.
FIELDING, P. E. & WHITE, T. J. (1987). *J. Mater. Res.* 2, 387-414.
KESSON, S. E. & WHITE, T. J. (1986a). *Proc. R. Soc. London Ser. A,* 405, 73-101.
KESSON, S. E. & WHITE, T. J. (1986b). *Proc. R. Soc. London Ser. A,* 408, 295-319.
KLUG, H. P. & ALEXANDER, L. E. (1974). *X-ray Diffraction Procedures,* 2nd ed., pp. 270-279. New York: Wiley-Interscience.
LIFSCHITZ, I. M. (1937). *Phys. Z. Sowjet.* 12, 623-643.
MIJLHOFF, F. C., IJDO, D. J. W. & ZANDBERGEN, H. W. (1985). *Acta Cryst.* B41, 98-101.
ROTH, R. (1981). Report NBSIR 81-2241. Annual Report, National Measurement Laboratory, Office for Nuclear Technology, Sydney, Australia.
WARREN, B. E. (1969). *X-ray Diffraction,* pp. 216-227. Reading, MA: Addison-Wesley.
WILSON, A. J. C. (1963). *Mathematical Theory of X-ray Powder Diffractometry,* pp. 1-53. New York: Gordon & Breach.
WILSON, A. J. C. & ZSOLDOS, L. (1965). *Proc. R. Soc. London Ser. A* 290, 508-514.